Earth and Planetary Science Letters 418 (2015) 136–148

Contents lists available at ScienceDirect

Earth and Planetary Science Letters

www.elsevier.com/locate/epsl

Composition of the slab-derived fluids released beneath the Mariana forearc: Evidence for shallow dehydration of the subducting plate

Julia M. Ribeiro [a,*], Robert J. Stern [a], Katherine A. Kelley [b], Alison M. Shaw [c], Fernando Martinez [d], Yasuhiko Ohara [e,f]

[a] Geosciences Department, University of Texas at Dallas, 800 W. Campbell Rd., Richardson, TX 75083-0688, USA
[b] Graduate School of Oceanography, University of Rhode Island, Narragansett Bay Campus, Narragansett, RI 02882, USA
[c] Department of Geology and Geophysics, Woods Hole Oceanographic Institution, Woods Hole, MA 02543, USA
[d] Hawai'i Institute of Geophysics and Planetology, SOEST, University of Hawai'i at Manoa, 680 East-West Rd, POST 602, Honolulu, HI 96822 USA
[e] Hydrographic and Oceanographic Department of Japan, 2-5-18 Aomi, Koto-ku, Tokyo 135-0064, Japan
[f] Japan Agency for Marine-Earth Science and Technology, Natsushima 2-15, Yokosuka 237-0061, Japan

ARTICLE INFO

Article history:
Received 10 June 2014
Received in revised form 4 December 2014
Accepted 13 February 2015
Available online 18 March 2015
Editor: T. Elliott

Keywords:
basalt
geochemistry
volatiles
Mariana arc
subduction zone
forearc rift

ABSTRACT

In cold subduction systems, the downgoing plate is thought to mostly dehydrate (≥90% water) beneath the arc front. However, the composition of aqueous fluids released from the shallow subducting slab is poorly constrained because the occurrence of melt inclusions is rare in forearcs. The Southeast Mariana Forearc Rift (SEMFR) is a recently discovered site where extensionally induced magmatism occurred in Pliocene time unusually close to the trench. SEMFR basalts sampled fluids derived from the subducted plate at ~30 to 100 km deep. Here, we use SEMFR basalts to obtain new insights into the composition of shallow slab-derived fluids by evaluating major element, trace element and volatile contents of olivine-hosted melt inclusions and glassy rinds. Olivine-hosted melt inclusions and their host glassy rinds both contain at least ~2 wt% H_2O, representing minimum estimates for magmatic water content. Melt inclusions have the highest volatile and alkali ratios (i.e., $H_2O/Ce = 6000–19000$; $Rb/Th = 200–2600$; $Cs/Th = 0.4–20$) yet recorded in glasses from subduction zones (arc magmas have mean $H_2O/Ce < 2700$; $Rb/Th < 40$; $Cs/Th < 2$). Our results indicate that shallow slab-derived fluids are water- and alkali-rich as compared to the deeper fluids released beneath the arc system. Shallow subduction outfluxes peak at ~70–80 km slab depth, demonstrating that significant slab dehydration occurs beneath the forearc.

1. Introduction

Subducting oceanic lithosphere and sediments (slab) carry fluids and volatiles from the Earth surface down into the mantle and recycle most of them back to the surface through arc magmatism. Aqueous fluids released from the breakdown of hydrous minerals from subducting slabs play a key role in subduction recycling. Fluids released from the slab at shallow depths promote serpentinization of the forearc mantle, but typically do not trigger melting due to low temperatures (Fryer et al., 1995; Hyndman and Peacock, 2003; Schmidt and Poli, 1998; Tatsumi, 1989). In contrast, deeper slab fluids interact with hot asthenospheric mantle to generate magmas beneath active arc volcanoes and backarc basin spreading centers (Gill, 1981; Grove et al., 2012; Schmidt and Poli, 1998).

Convergent margin magmas capture slab-derived fluids and retain these geochemical signatures better than serpentinites because magma can be trapped as olivine-hosted melt inclusions and as quenched rims on pillow basalts. Quenched, glassy melt inclusions in particular may preserve the chemical imprint of their subduction components (e.g., Kent, 2008; Ruscitto et al., 2012; Shaw et al., 2008), as their host mineral can protect them from alteration and low pressure degassing (e.g., Schiano, 2003). Melt inclusions also provide snapshots of the melt evolution during crystallization; and because olivine fractionates early in basaltic systems, their melt inclusions can record early stages of magmatic processes (e.g., Kelley et al., 2010).

Recent thermal models along with estimates of the dehydration efficiency of global subduction zones suggest that the downgoing plate in cold subduction systems such as the Mariana system can retain mineral bound-water to depths >80 km before mostly

* Corresponding author.
E-mail address: juliaribeiro@utdallas.edu (J.M. Ribeiro).

http://dx.doi.org/10.1016/j.epsl.2015.02.018
0012-821X/

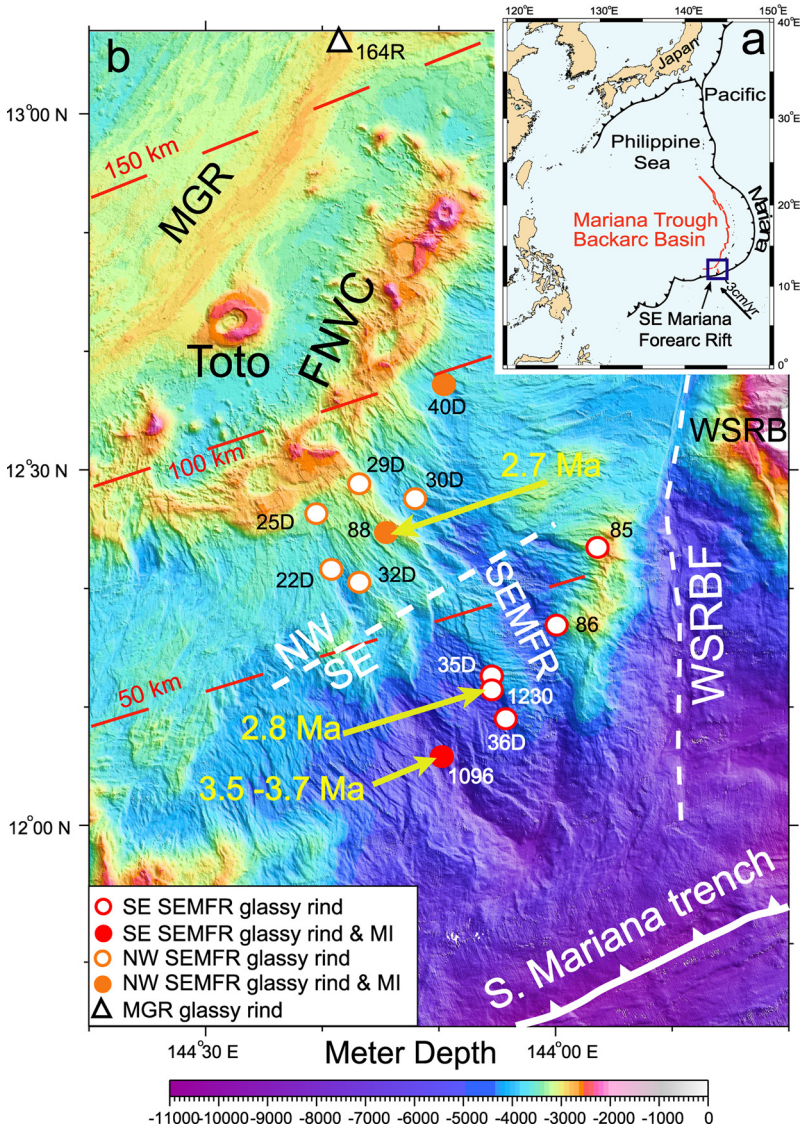

Fig. 1. Locality maps and sketch showing the plate tectonic setting of samples in this study. a) Location of the Mariana intraoceanic arc system in the Western Pacific. The arrow represents convergence direction and rate (Kato et al., 2003). The blue box shows the area of b. b) Detailed bathymetric map of the Southeast Mariana Forearc Rift (SEMFR) in the southeastern Mariana arc. SEMFR is divided into SE and NW sectors, separated by a thick white dashed line. Numbers with D indicate TN273 dredging sites; other numbers represent sampling sites for JAMSTEC Yokosuka (YK08-08 Leg 2 and YK10-12) and Kairei (KR00-03 Leg 2) cruises. Large yellow numbers are ^{40}Ar–^{39}Ar ages (Ribeiro et al., 2013b). Toto: Toto caldera, FNVC: Fina Nagu volcanic chain, WSRBF: West Santa Rosa Bank Fault, MGR: Malaguana-Gadao Ridge. The thin red dashed lines with numbers denote approximate depths to the subducted Pacific plate (Becker, 2005). Map generated with GMT (Smith and Wessel, 1990; Wessel and Smith, 1995, 1998) using a compilation from the University of New Hampshire/Center for Coastal and Ocean Mapping/Joint Hydrographic Center. (For interpretation of the references to color in this figure legend, the reader is referred to the web version of this article.)

dehydrating beneath the arc volcanoes (Van Keken et al., 2011; Wada et al., 2008). Mass balance calculations indicate that less than 10% of subducted water is available to be recycled deeper into the lower mantle (Shaw et al., 2012, 2008; Van Keken et al., 2011). Shallow dehydration of the subducting plate is central in assessing the fluid budget; yet, we can rarely sample such shallow subduction fluids released beneath forearcs despite their importance.

Forearc rifts can provide critical insights into shallow subduction processes because they may erupt basalts unusually close to the trench (Ribeiro et al., 2013b). Such basalts form by decompression melting of the asthenospheric mantle wedge fluxed by shallow slab-derived fluids (Ribeiro et al., 2013a). Identifying and examining forearc rift basalts and their olivine-hosted melt inclusions thus provides a unique opportunity to investigate the composition of shallow slab-derived fluids. Here, we report results from studying olivine-hosted melt inclusions and glassy rims from young basalts erupted from a forearc rift in the southern Mariana convergent margin and use these results to advance our understanding of shallow slab-derived fluid compositions. We present major element, volatile (H_2O, CO_2, S, Cl, F) and trace element contents of their olivine-hosted melt inclusions and glassy pillow rinds. We use this new dataset to constrain the composition of aqueous fluids released from the shallow subducted slab and explore how such fluids have triggered flux melting of shallow hot mantle unusually close to the trench. We show that the shallow subduction component is enriched in water and alkalis relative to the fluids released deeper. We find that the contribution of shallow water-rich fluids becomes most important when the slab is ~70–80 km depth, indicating that the downgoing plate significantly dehydrates beneath the forearc.

2. Geological setting

The Mariana convergent margin results from subduction of the Pacific Plate beneath the Philippine Sea Plate (Fig. 1a; Meijer and

Reagan, 1981). To the south, the Mariana Trench curves from N–S to E–W to accommodate collision with the Caroline Ridge (Fujioka et al., 2002), where it reaches the deepest point on Earth's surface at the Challenger Deep (10 994 m; Gardner and Armstrong, 2011). Most of the Mariana forearc formed when subduction began in the Eocene ~52 Ma ago (Ishizuka et al., 2011; Reagan et al., 2013), but collision of the Caroline Ridge has required the southernmost Mariana forearc to stretch since ~5 Ma to accommodate opening of the Mariana Trough backarc basin (the Malaguana-Gadao Ridge, MGR; Fig. 1), opening a forearc rift named the SE Mariana forearc rift (SEMFR). Forearc extension was accompanied by eruption of basalts, probably accompanying seafloor spreading 2.7–3.7 Ma ago (Ribeiro et al., 2013b) that have rapidly become a diffuse magmatic system (Martinez et al., 2014). SEMFR is now broadly deformed by post-magmatic extension characterized by NNW-trending rifts and grabens. Today, the forearc rift extends from the trench to the Fina–Nagu Volcanic Chain (i.e., 30 to 80 km from the trench), and it is ~40 km wide and at least 60 km long (Fig. 1b). Geology and morphology of the forearc rift vary along it. Relief near the trench is rugged and affected by normal faulting and landsliding, whereas near the arc, the forearc rift has smoother relief with better-preserved pillow outcrops (Ribeiro et al., 2013b). Details for the analytical methods are reported in Appendix Tables A1 and A2.

3. Methods

Major elements, trace elements and major volatile concentrations (H_2O, CO_2, F, S, Cl) of 20 naturally glassy olivine-hosted melt inclusions were analyzed along with the volatile compositions of 13 naturally-quenched pillow rinds from SEMFR basalts. We also report the volatile contents of one sample collected along the Malaguana-Gadao Ridge during JAMSTEC Kairei cruise KR00-03 Leg 2, Kaiko dive 164. Details for the major element and trace element analyses of the glassy rinds were previously reported (Ribeiro et al., 2013a). Details for the analytical methods are reported in Appendix Tables A1 and A2.

3.1. Analytical methods

Samples were crushed and sieved with 2 mm, 1 mm, 0.5 mm mesh screens. Fresh, brown and translucent glass chips from pillow rinds and fully enclosed olivine-hosted melt inclusions were handpicked and examined under a microscope to ensure that translucent, brown or clear crystal-free glass was available for analysis (Fig. 2a). Glasses were mounted in indium metal and polished on a single side (Fig. 2b) for ion- and electron-probe analyses. Analyzed melt inclusions are sub-rounded (diameter >20 μm), fully enclosed by their olivine host and generally associated with a gas bubble. Volatiles were measured using the CAMECA Secondary Ion Mass Spectrometer 1280 at Woods Hole Oceanographic Institution, with a 1.28 nA and 30 μm beam of Cs^+, following the technique outlined in Hauri et al. (2002). Melt inclusions <30 μm were measured using a 500 pA and 20 μm beam. Calibration curves of 10 glass standards (519-4-1, 51-3, 46D, 1649-3, D20-3, JD17H, 1654-3, 6001, D52-5, NS-1; see Appendix Table A2 for details) yield $r^2 \geq 0.99$ for all volatiles, but for CO_2 ($r^2 > 0.92$). Sample replicates yield one standard deviation (1σ) ≤ 0.2 wt% for water and ≤300 ppm for the other volatiles, and a reproducibility ≤10% rsd. Details and tables for major and trace elements of the glassy rinds were previously reported by Ribeiro et al. (2013a).

Major element compositions of the olivine-hosted melt inclusions were measured using the JEOL JXA-8200 Superprobe at the Massachusetts Institute of Technology, using a 10 μm defocused beam to minimize alkali loss, a 15 kV accelerating voltage and a 10 nA beam current. The glass standard ALV-1690-20 and olivine standard P140 of Grove et al. (1992) were analyzed daily for calibrations. Precision is ≤0.3% and the standard deviations (1σ) of repeated analyses of the unknowns are ≤0.5% for the melt inclusions and ≤1.1% for the olivine. Repeated analyses of the glass standard gave a mean CaO = 10.85 wt%,

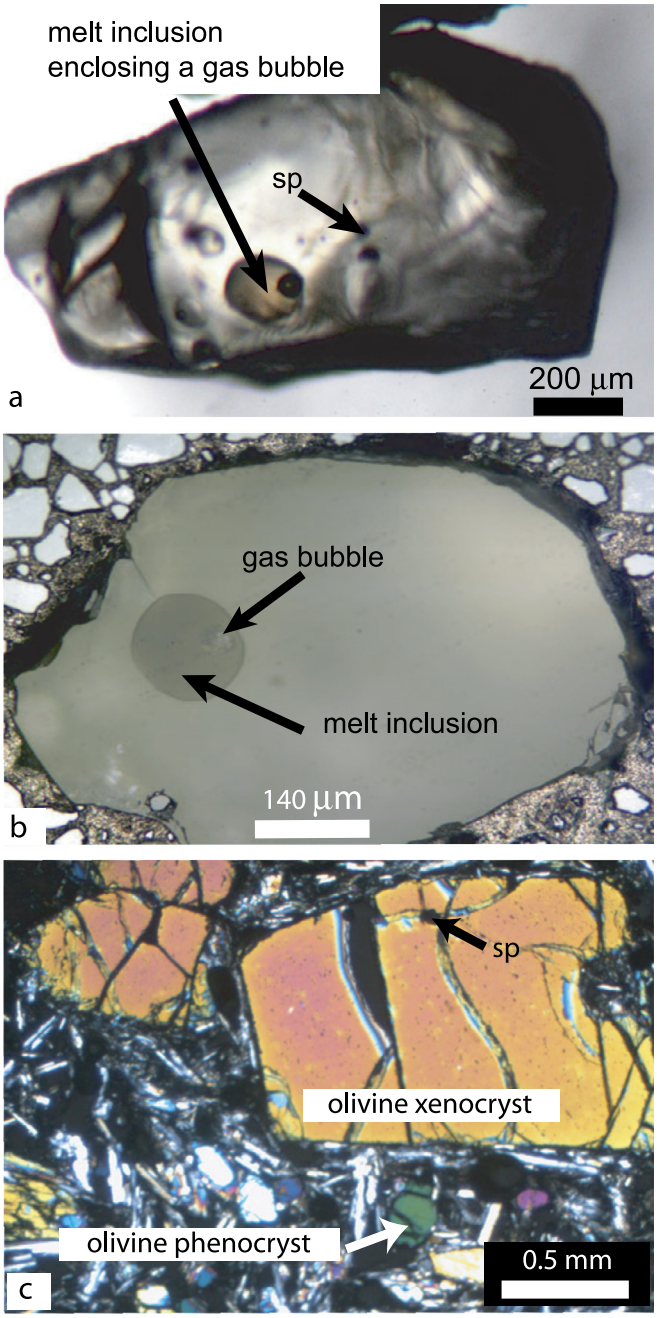

Fig. 2. a), b) Microphotographs of olivine-hosted melt inclusions. a) Unpolished olivine in a 70% propanol bath. This method allows us to see through the olivine and to look at the melt inclusion. The dark circle inside the melt inclusion is a shrinkage bubble formed in reason of the greater expansion of the silicate melt than the olivine host during cooling (Schiano and Bourdon, 1999). Olivine also encloses some chromium spinel (sp) inclusions. No secondary melt inclusions occurring as trails along cracks were observed, demonstrating that SEMFR olivine xenocrysts are neoblasts that trapped the melt inclusions during olivine growth (Andersen and Neumann, 2001). b) Polished olivine with melt inclusion pushed into indium (grey material surrounding the olivine) for SIMS analyses. c) Microphotograph of the larger olivine xenocrysts (1–2 mm), with their reaction rim, surrounded by smaller groundmass olivines (Ribeiro et al., 2013b). Microphotograph (a) was taken with a binocular microscope and microphotographs (b) and (c) were taken under a polarized microscope.

Al_2O_3 = 15.51 wt%, K_2O = 0.15 wt%, MnO = 0.19 wt%, Na_2O = 3.13 wt%, TiO_2 = 1.71 wt%, SiO_2 = 49.90 wt%, P_2O_5 = 0.18 wt%, FeO = 9.91 wt%, MgO = 7.68 wt%. Olivine hosts were analyzed 3–4 times from the core to the rim to ensure that no reverse zoning occurred.

Trace element analyses were carried out at the University of Rhode Island with a UP-213 Nd-YAG Laser Ablation System coupled to a Thermo X-series II quadrupole Inductively Coupled Plasma Mass Spectrometer. Melt inclusions were ablated using a 5 Hz repeat rate, 60% pulse beam energy and 20–80 μm spot size (Kelley et al., 2003). Spectra were normalized to ^{43}Ca as the internal standard. Calibration curves use 8 standards (BHVO-2G, BCR-2G, BIR-1G, GOR 132, StHIs, T1, ML-3B, KL2; Jochum et al., 2006; Kelley et al., 2003) analyzed under the same conditions as the unknowns and using an 80 μm spot size. Calibration curves yield $r^2 \geq 0.999$ relative to the reported standard values, but for Zn, Co, Tb, Yb, U and Lu ($r^2 \geq 0.996$). Reproducibility of replicate analyses are ≤3% rsd for Sr, Nb, Rb, Ba, K_2O, ≤5% rsd for Y, Li, U, and ≤11% rsd for Th and Ni. Rare Earth element (REE) patterns of the melt inclusions are smooth and their Heavy REE (HREE) patterns are subparallel to their host glass (Appendix Fig. A1).

3.2. Melt inclusion composition corrections

Melt inclusion compositions were corrected for post-entrapment crystallization (PEC). Olivine can crystallize on melt inclusion walls after entrapment, depleting the inclusion in Mg and enriching it in Fe, volatiles, and other incompatible elements (Kent, 2008). Post-entrapment crystallization can be accounted for by calculating the Fo content of the olivine that should be in equilibrium with the melt inclusion using a partition coefficient ($K_D^{ol\text{-}liq}$[Fe/Mg]) of 0.3 (Roeder and Emslie, 1970), and by comparing the Fo equilibrium to the measured Fo content of the host olivine near the melt inclusion (Appendix Fig. A2). PEC is characterized by Fo-equilibrium < Fo-measured and can be corrected by adding back equilibrium olivine to the melt inclusion composition in 0.1% increments until the host olivine composition is reached. This correction is sensitive to the ratio Fe^{3+}/Fe_T in the melt inclusions. While this ratio is not known for SEMFR lavas, we previously used $Fe^{3+}/Fe_T = 0.17$ (Kelley and Cottrell, 2009) because SEMFR lavas have a backarc-like geochemical imprint (Ribeiro et al., 2013a, 2013b). For consistency, we used similar ratios for the olivine-hosted melt inclusions and the glassy rinds. The effect of varying the Fe^{3+}/Fe_T from 0.17 (average BABB value) to 0.25 (average arc value) on the PEC correction is minor for most of the major elements ($1\sigma < 0.5$ wt%). Such variation decreases the percentage of olivine added by 5% (see Appendix B for details) and it increases Mg# of the melt inclusion ($1\sigma < 2\%$). Major element and volatile contents in all the melt inclusions were PEC corrected (Appendix Fig. A2); and less than 20% equilibrium olivine was added back to the composition of the melt inclusion (mean = 13.0 ± 5.7%; Appendix Table A4). To ensure that the melt inclusion compositions faithfully represent the original composition of the primary melt, we investigated the effect of PEC over-correction on the composition of the melt inclusions. The lack of relationship between the percentage of olivine added and the composition of the melt inclusion in Fe_8, Mg#, MgO content and H_2O/Ce ratio (Appendix Figs. B1, B2) indicates that the compositions of the melt inclusions are not over-corrected for olivine PEC. Details are reported in Appendix B. Uncorrected and corrected major element, trace element and volatile contents of the olivine-hosted melt inclusions and glassy rinds are reported in Appendix Tables A3 and A4.

4. Results

4.1. Volatile contents

Volatile contents of SEMFR glassy rinds show a wide range in CO_2 (16–132 ppm), F (90–276 ppm), S (138–1127 ppm) and Cl (299–1401 ppm) concentrations. Water contents of SEMFR glassy rinds are more homogeneous, from 1.2 to 2.4 wt%. PEC-corrected melt inclusions have a wider range of CO_2 (27–539 ppm) and H_2O (0. 37–2.3 wt%) concentrations (Fig. 3; Appendix Table A4). In contrast, F (38–136 ppm), S (36–963 ppm) and Cl contents (76–637 ppm) show a smaller compositional range as compared to the glassy rims (Fig. 3). Averaged water content of SEMFR glassy rinds (1.96 ± 0.30 (1σ) wt% H_2O) and melt inclusions (1.76 ± 0.42 (1σ) wt% H_2O) are similar within their one standard deviation error, although the melt inclusions contain higher CO_2 contents. The MGR glassy rind sample has volatile contents (CO_2 = 17 ppm; H_2O = 2.14 wt%, S = 274 ppm, Cl = 971 ppm) that fall within the compositional range of the SEMFR glass, with the exception of F (368 ppm).

4.2. Major element composition of glass and host olivine

SEMFR glassy rinds are low-K basalts to basaltic andesites (51.17–56.75 wt% SiO_2; Fig. 4a; Ribeiro et al., 2013a). PEC-corrected SEMFR melt inclusions are less evolved than their host glassy rinds, ranging from low-K basalts to low-K basaltic andesites (48.94–53.11 wt% SiO_2). The less fractionated nature of SEMFR melt inclusions is also seen in Mg# (= 100 × Mg/[Mg + Fe_T]), with Mg# = 70.6–79.6 for melt inclusions and Mg# = 38.0–61.4 for the glassy rinds (Fig. 4b). These results indicate that the melt inclusions trapped more primitive melts than the associated host glassy rinds.

Major element contents of PEC-corrected SEMFR melt inclusions and glassy rinds plotted against MgO do not overlap (Fig. 4c–d). Plots of CaO against MgO show that SEMFR melt inclusions plot on the high-MgO side of plagioclase fractionation-controlled kinks in the compositional trends, at MgO ~7 wt% and CaO ≥11 wt% (Fig. 4c), demonstrating that the melts sampled by the melt inclusions have only crystallized olivine.

The compositional variations of the olivine-hosted melt inclusions cannot be solely explained by olivine fractionation. Indeed, the melt inclusions have silica contents ranging from 49 to 53 wt% and MgO contents varying from 9 to 14 wt% with the lack of corresponding variations in Mg# (70–80) and TiO_2 (Fig. 4b, d), suggesting that the melt inclusions trapped different primary melts produced from various degrees of mantle melting. In addition, the CaO-rich and high-Mg# nature of the melt inclusions suggest that the melt inclusions were in equilibrium with depleted harzburgitic residues.

4.3. Trace elements

Rare Earth Element (REE) patterns of olivine-hosted melt inclusions for NW and SE SEMFR are MORB-like, depleted in Light REE (LREE; $[La/Yb]_N < 1$; $[La/Sm]_N < 1$; $[Gd/Yb]_N = 1$) with no europium anomaly ($[Eu/Eu^*]_N = 1$; Fig. 5a). Trace element patterns of the melt inclusions have positive anomalies in fluid-mobile elements (Ba, Cs, Rb, K, Sr, U, Pb) and negative anomalies in High Field Strength Elements (HFSE: Nb, Zr, Ti, La, Ce, Th; Fig. 5b). Glassy rim compositions are generally enriched in LREE relative to olivine-hosted melt inclusions, but the least LREE-depleted REE patterns and the least HFSE-depleted trace element patterns of NW SEMFR melt inclusions overlap the most LREE- and HFSE-depleted patterns of host lava glassy rims. All spider diagrams for NW SEMFR melt inclusions have fluid-mobile element contents that are similar

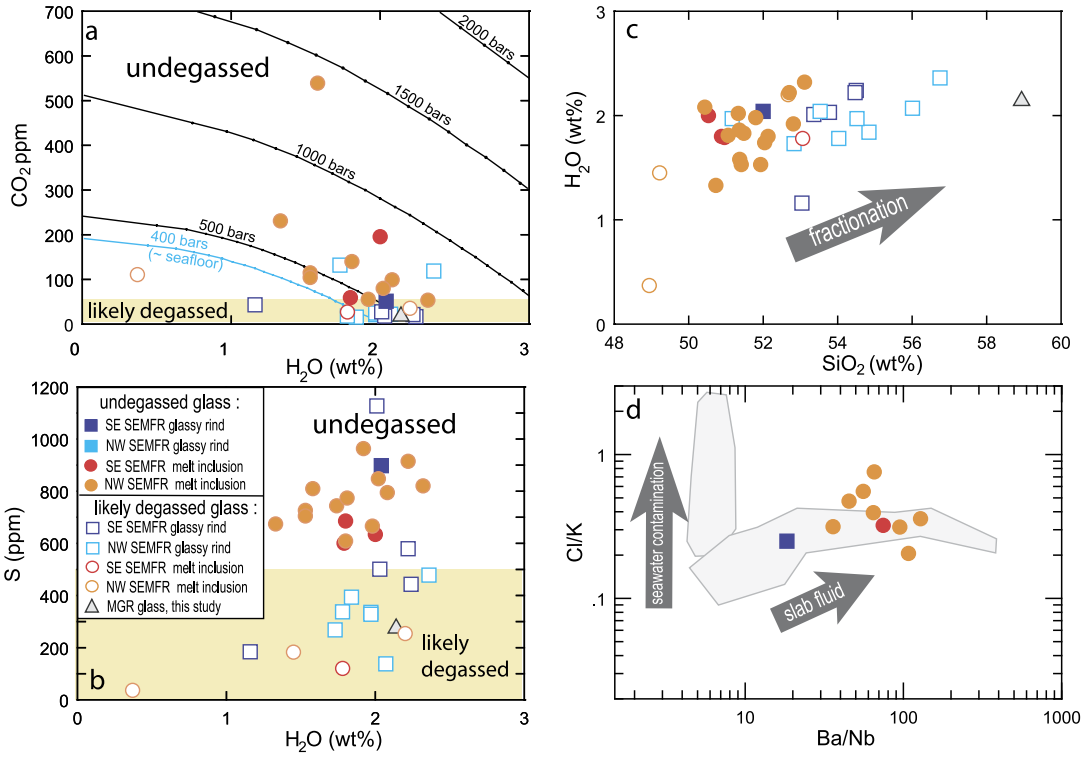

Fig. 3. Volatile contents of SEMFR glassy rinds and melt inclusions. a) H_2O vs. CO_2 diagram. The yellow field identifies samples with $CO_2 < 50$ ppm, which are likely to have degassed some H_2O. Isobars were calculated using the VolatileCalc vapor solubility model for basalt compositions (Newman and Lowenstern, 2002). The blue saturation curve shows the approximate depth of SEMFR seafloor. b) H_2O vs. S diagram. The yellow field identifies the likely degassed samples with $S < 500$ ppm. c) Effect of crystal fractionation on the water contents of the SEMFR glasses. As fractionation occurs, the melt become enriched in silica and water. d) Cl/K vs. Ba/Nb diagram of Kent et al. (2002) used to discriminate the effect of seawater alteration vs. slab-derived fluids in SEMFR glasses. The lack of clear positive correlation of Cl/K with the subduction proxy suggests that the composition of SEMFR glasses may be affected by assimilation of Cl-rich material. We also report the compositional field (in grey) of the Lau Basin glasses (Kent et al., 2002) for comparison. (For interpretation of the references to color in this figure legend, the reader is referred to the web version of this article.)

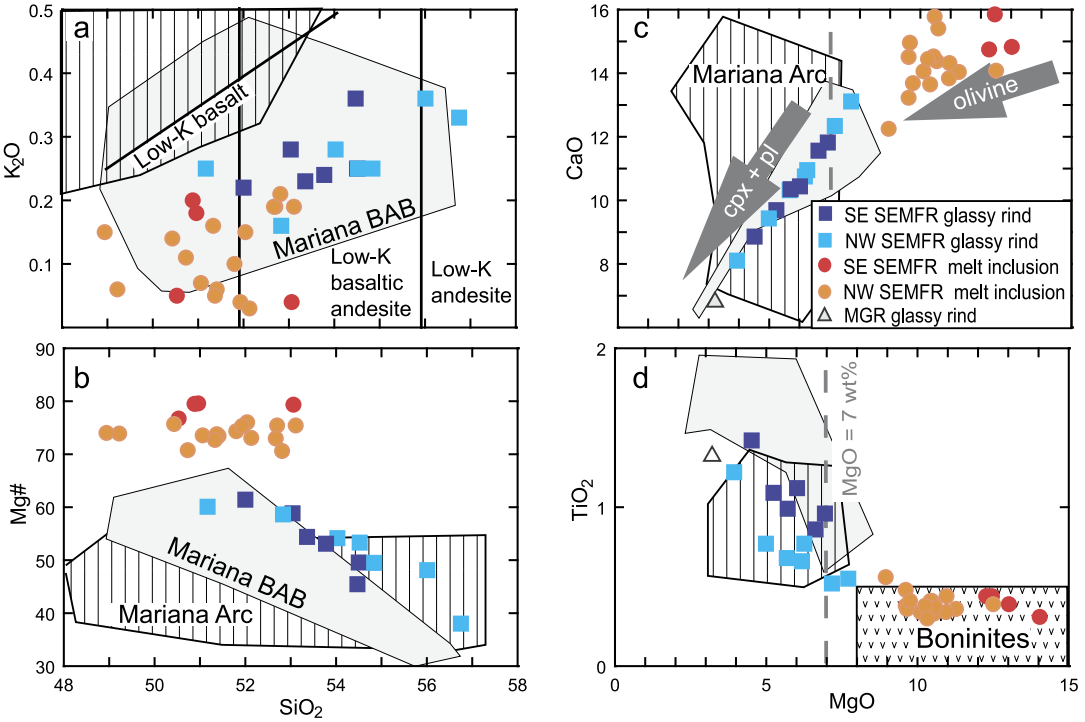

Fig. 4. Major element variation diagrams (all data recalculated to 100% anhydrous) for SEMFR glassy rinds and melt inclusions. Melt inclusion data are corrected for post-entrapment olivine crystallization. a) K_2O vs. SiO_2 diagram, with fields after Peccerillo and Taylor (1976). b) Mg# vs SiO_2 (Mg# $= 100 \times Mg/[Mg + Fe]$) showing that the melt inclusions are more primitive (Mg# > 70) than glassy rinds (Mg# < 70). c) CaO, d) TiO_2 vs. MgO diagrams for SEMFR glassy rinds and olivine-hosted melt inclusions, and MGR glassy rind (black triangles). Arrows represents fractionation trends. The grey dashed line highlights the hinge in CaO, resulting from plagioclase and clinopyroxene crystallization starting at MgO = 7 wt%. Melt inclusions have MgO > 7 wt% demonstrating that they crystallized olivine only. Cpx: clinopyroxene, pl: plagioclase. The field for boninites is from Le Bas (2000).

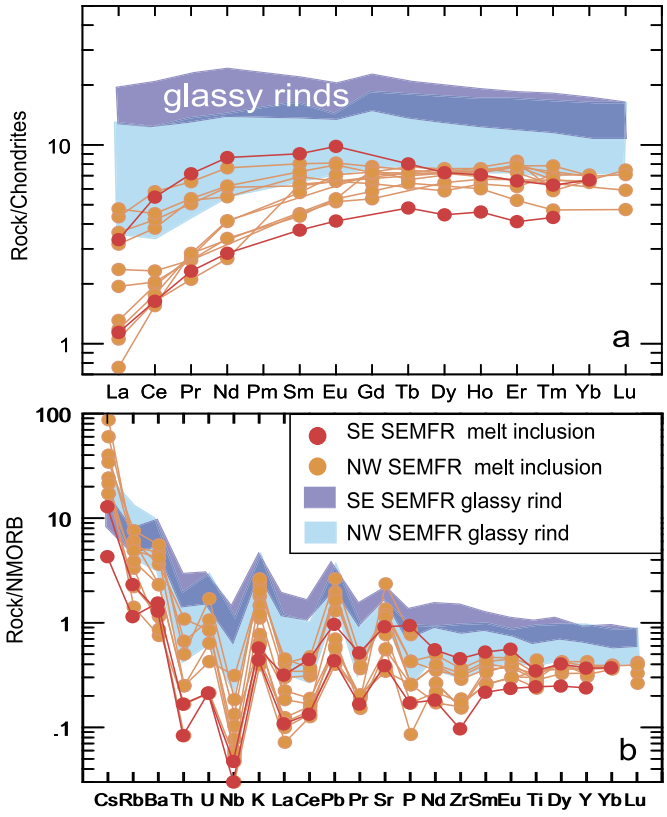

Fig. 5. (a) Chondrite-normalized (Sun and McDonough, 1989) rare earth element (REE) patterns and (b) N-MORB normalized (Sun and McDonough, 1989) trace element patterns of SEMFR lavas from the NW and the SE sectors. REE patterns of the host glass are flat to slightly depleted in LREE (blue compositional field). SE SEMFR melt inclusions are more depleted in LREE and in HFSE than their host glass. NW SEMFR melt inclusions are as depleted as to more depleted in HFSE and in LREE than their host glassy rinds. See text for details.

to or higher than their host basalt glassy rims (Fig. 5b). In contrast, the REE and trace element patterns of SE SEMFR melt inclusions do not overlap those of their host glass (Fig. 5a).

The lower LREE abundances and the greater HFSE depletions also suggest that NW and SE SEMFR melt inclusions were produced from a more depleted mantle source than were their host basalts. Variations in SEMFR melt inclusion REE patterns (Fig. 5), ranging from LREE-depleted to nearly flat, and their moderate to strong Nb depletions, suggest that the melt inclusions reflect magma batches formed from different degrees of mantle depletion and/or various extents of melting, as also shown by their major element contents. Chemical differences between SE and NW SEMFR lavas (Ribeiro et al., 2013a) are also observed in the trace element patterns of their melt inclusions. SE and NW SEMFR melt inclusions show similar HSFE depletions and their trace element patterns mostly overlap, but NW SEMFR inclusions are more enriched in Cs, as also observed for their glassy rinds (Fig. 5).

5. Discussion

SEMFR melt inclusions and their host glassy rinds have distinctive major and trace element compositions with both MORB-like (e.g., major element compositions and REE patterns) and arc-like (e.g., water and fluid-mobile element contents) geochemical features. SEMFR melt inclusions have the lowest TiO_2, FeO* and Na_2O contents and the highest MgO and CaO contents recorded in the Mariana intraoceanic arc-backarc basin system (Fig. 4), along with a strong depletion in HFSE and LREE relative to their associated glassy rinds (Fig. 5). These results suggest that, compared to host basalts, SEMFR melt inclusions sampled more depleted melts that formed from higher degrees of melting of a mantle source fluxed by subduction components.

In the following discussion, we use our SEMFR glassy dataset to characterize shallow subduction inputs. First, we address 3 key questions to ensure the robustness of our measurements: (i) have these volatile concentrations been affected by degassing and re-equilibration processes?; (ii) have chlorine contents been affected by assimilation processes?; and (iii) what are the least-degassed volatile contents of SEMFR magmas? Then, we interpret the significance of our dataset by discussing the genesis of the olivine-hosted melt inclusions and constraining the composition of shallow slab-derived fluids.

5.1. Magmatic degassing, water re-equilibration and assimilation effects on volatile contents in SEMFR glasses

An important question is whether the volatile contents of the melts faithfully record the volatile contents of their sources (mantle and subduction inputs), or whether volatile contents of the melts have been compromised by degassing, re-equilibration and/or assimilation processes of chlorine-rich material (i.e., seawater, seawater-altered crust or brines) during magma ascent, storage or eruption (Kent et al., 2002).

5.1.1. Magmatic degassing

While melt inclusions are fully enclosed by their olivine hosts, preventing post-entrapment degassing, olivines might have trapped melt that had already degassed. The effects of degassing is assessed by examining co-variations of volatiles with differing melt-vapor solubility, such as H_2O, S and CO_2 contents of the melt inclusions and host glassy rinds. CO_2 solubility is pressure-dependent and in basaltic magmas it drastically decreases with decreasing pressure relative to water (e.g., Dixon and Stolper, 1995), so that CO_2 will exsolve first from the melt upon decompression. The vapor–melt partitioning of sulfur is complex and strongly dependent of temperature, pressure, oxygen fugacity, sulfur fugacity and melt composition. Experiments on mafic melts show that sulfur is preferentially incorporated into the vapor phase (Scaillet and Pichavant, 2003; Webster and Botcharnikov, 2011). Such results are consistent with the empirical covariations of water and sulfur suggesting that sulfur solubility in basaltic magmas is intermediate between water and CO_2 solubilities (Sisson and Layne, 1993; Wade et al., 2006). Our dataset was thus screened for minimally degassed volatile contents, following the approach of Kelley et al. (2010) and Shaw et al. (2008), (i) using CO_2 and S thresholds and (ii) comparing melt–vapor saturation and eruption pressures. For the first evaluation, glassy rinds and PEC-corrected melt inclusions with $CO_2 > 50$ ppm and $S \geq 500$ ppm are considered to have retained enough CO_2 and S so that H_2O was not significantly degassed. Based on this filter, most of the glassy rinds may have lost magmatic water by degassing (Fig. 3a–b), whereas most melt inclusions did not (Appendix Table A4).

Olivine-hosted melt inclusions can re-equilibrate to the vapor-saturated water content of their host magma at crustal depth (Plank et al., 2013). Indeed, hydration–dehydration experiments on olivine-hosted melt inclusions show that they can gain or lose water via rapid diffusive re-equilibration of H^+ (protons) and metal vacancies through the host olivine upon ascent (e.g., Bucholz et al., 2013; Gaetani et al., 2012; Hauri, 2002). Re-equilibration will re-

Table 1
Averages of minimally degassed, PEC-corrected volatile and trace element abundances in worldwide arc samples, SEMFR glassy rinds and SEMFR olivine-hosted melt inclusions.

Samples	Number of samples (n)	H_2O (wt%)	CO_2 (ppm)	F (ppm)	S (ppm)	Cl (ppm)	Rb (ppm)	Nb (ppm)	Cs (ppm)	Ba (ppm)	Ce (ppm)	Th (ppm)	H_2O/Ce	Cl/Nb	Rb/Th	Cs/Th	Ba/Th	Slab depth (km)	H_2O-max (wt%) Plank et al. (2013)	1σ	H_2O-25% (wt%) Plank et al. (2013)	1σ
Central America arc	$n=87$	3.47	300	486	1743	1202	16.7	4.8	0.4	451	26	1.56	2524	437	12	0.5	576	118	3.63	*0.11*	3.60	*0.09*
1σ		*0.70*	*159*	*406*	*693*	*424*	*14.5*	*6.7*	*0.2*	*228*	*33*	*2.42*	*2168*	*265*	*4*	*0.1*	*447*	44	*0.96*		*0.94*	
Antilles arc	$n=116$	1.81		374	1212	1389	9.9	4.2	0.3	130	16	1.04	1672	486	11	0.4	103	141				
1σ		*1.28*		*246*	*628*	*566*	*3.3*	*4.5*	*0.2*	*72*	*9*	*0.55*	*1349*	*305*	*4*	*0.2*	*32*	1				
Mexico arc	$n=168$	2.58	1049		1438	970	11.6	8.7	0.3	279	31	1.19	1150	218	12	0.3	296	85				
1σ		*1.26*	*836*		*553*	*274*	*4.9*	*10.8*	*0.1*	*194*	*22*	*0.93*	*834*	*178*	*4*	*0.1*	*135*	28				
Cascades arc	$n=129$	1.83	625	469	1508	637	10.4	6.4		283	33	1.14	696	218	10		298	90	3.19	*0.96*	3.45	*1.15*
1σ		*0.88*	*280*	*393*	*900*	*281*	*3.5*	*4.2*		*133*	*11*	*0.37*	*449*	*409*	*3*		*77*	10	*1.20*		*0.90*	
Aleutians–Alaska arc	$n=181$	3.33	208	373	2787	1968	17.0	2.3	0.7	296	18	1.68	1808	845	11	0.5	177	95	3.82	*0.35*	3.53	*0.14*
1σ		*1.54*	*158*	*163*	*1577*	*1220*	*7.9*	*1.7*	*0.4*	*130*	*6*	*0.66*	*1032*	*800*	*2*	*0.3*	*34*	10	*1.60*		*1.50*	
Tonga arc	$n=57$						6.4	0.3	0.3	119	6	0.17			37	1.6	705	94	3.76		3.47	
1σ							*1.7*	*0.1*	*0.2*	*22*	*3*	*0.05*			*11*	*1.0*	*154*	10	*0.70*	*0.60*		
Kamchatka arc	$n=51$	3.16	906	611	1815	676	11.9	1.5		266	14	2.55	2623	380	5		142	111	4.13	*0.69*	3.72	*0.40*
1σ		*1.10*	*354*	*385*	*449*	*213*	*2.1*	*0.4*		*69*	*3*	*0.87*	*535*	*132*	*1*		*118*	34	*1.70*		*0.85*	
Mariana arc	$n=170$	3.48	500	485	1265	678	10.7	1.1	0.3	156	13	0.66	2650	595	15	0.4	293	169	4.50	*0.72*	4.22	*0.52*
1σ		*1.20*	*541*	*500*	*446*	*367*	*5.7*	*0.6*	*0.2*	*79*	*6*	*0.38*	*1446*	*445*	*4*	*0.2*	*193*	6	*1.04*	*1.00*		
MORB	$n=678$	0.16	547	128	1077	56	3.66	8.5	0.0	39	10.0	0.44	160	7	8	0.1	89					
1σ		*0.03*	*301*	*44*	*151*	*29*	*6.32*	*5.1*	*0.1*	*66*	*6.2*	*0.72*	*104*	*5*	*20*	*0.2*	*209*					
SE SEMFR glassy rinds	$n=6$	2.04	51	186	898	447	3.7	1.9	0.1	47	9	0.24	2366	239	17	0.4	208	45				
1σ							*0.8*	*0.6*	*0.0*	*12*	*2*	*0.07*	$n=1$	$n=1$	*5*	*0.2*	*58*	*8*				
NW SEMFR glassy rinds	$n=7$						4.3	1.0	0.1	40	5	0.14			35	1.2	314	75				
1σ							*1.5*	*0.8*	*0.0*	*13*	*2*	*0.07*			*14*	*0.7*	*100*	*6*				
SE SEMFR MI	$n=4$	1.86	127	115	640	427	1.0	0.1	0.1	9	2	0.02	5980	1012	70	4.4	581	45				
1σ		*0.12*	*96*	*22*	*43*	*278*	*0.5*	*0.0*	*0.0*	*1*	*2*	*0.01*			*53*	*3.9*	*126*	*8*				
NW SEMFR MI	$n=16$	1.83	158	81	773	304	2.4	0.3	0.3	17	2	0.05	11956	1462	82	6.8	509	75				
1σ		*0.29*	*153*	*14*	*101*	*144*	*1.1*	*0.2*	*0.2*	*11*	*1*	*0.04*	*4184*	*622*	*38*	*5.6*	*222*	*6*				

Grey numbers in italic are one standard deviations. Averaged slab depth for arc volcanoes is from Ruscitto et al. (2012).
MI: melt inclusions. See text and Appendix Tables A3 and A4 for details about composition of SEMFR glasses. SE SEMFR is near the trench and NW SEMFR is near the arc volcanoes (Fig. 1B).
SEMFR slab depth was extrapolated by using the South Mariana slab depth (Becker, 2005) reported in Fig. 1B.
H_2O-max corresponds to the averaged water content calculated by Plank et al. (2013) using the maximum water content in each volcano.
H_2O-25% represents the averaged water content for the top quartile of the water contents, screened for $S > 500$ ppm (Plank et al., 2013). Our averaged water contents of the worldwide arc glasses are similar to the water estimates of Plank et al. (2013) with $1\sigma \leq 1$ wt%.

set the water content of the melt inclusion to the water content of the ambient magma, but not the CO_2 content. The matching water concentrations of the melt inclusions in olivine crystals and host pillow-rind glasses suggests that re-equilibration occurred and the analyzed water contents represent minimum estimates (Bucholz et al., 2013; Gaetani et al., 2012). However, re-equilibration will drive water loss without any effect on the major and trace element contents. Thereby, covariation of the water content with major elements (Fig. 3c) suggests that water is controlled by crystal fractionation. Also, the relationship between H_2O/Ce and the subduction proxies (e.g., Rb/Th, Cs/Th; see Section 5.3) is difficult to be explained by re-equilibration processes and suggests that slab fluxes drives the water content of the SEMFR melt inclusions (Plank et al., 2013).

We also calculated the melt-vapor saturation pressure of each sample by using the mixed phase vapor saturation model VolatileCalc of Newman and Lowenstern (2002) for the system basalt–H_2O–CO_2. Because the solubility of volatiles in silicate melts decreases with decreasing pressure, low-pressure melts become oversaturated in volatiles and degas upon eruption. Thus, glasses with calculated saturation pressures lower than or equal to their collection (eruption) depths likely degassed CO_2 and possibly some H_2O. Most SEMFR glassy rinds give saturation pressures (225–806 bars; mean = 475 ± 136 (1σ) bars; Appendix Table A4) that approximate their collection depth 3090–5737 m (303–563 bars; mean = 388 ± 73 (1σ) bars) and thus were vapor-saturated when they erupted (Fig. 3a). In contrast, SEMFR melt inclusions are mostly vapor-oversaturated at the depth of collection, as they record saturation pressures from 255–1389 bars (mean = 607 ± 266 (1σ) bars; Appendix Table A4) that are mostly greater than those expected from their collection depths. These results are consistent with the trapping of melt inclusions at higher pressures (e.g., within a crustal magma chamber) relative to the matrix glasses.

5.1.2. Assimilation of Cl-rich material

Assimilation of seawater or seawater-altered crust by magma can affect volatile contents, especially Cl, as seawater has high Cl and low F contents (Cl = 19 500 ppm, F = 1.3 ppm). However, chlorine enrichment by this mechanism in the glassy rinds and melt inclusions can be ruled out, because the Cl and F contents of the SEMFR glasses (Cl = 76–1401 ppm, F = 38–276 ppm) differ strongly from that of seawater (Straub and Layne, 2003). Assimilation of chlorine-rich material prior to melt entrapment and quenching can also modify the chlorine content. To ensure that the chlorine content of the glasses faithfully reflects the addition of the subducted component, we compare the Cl/K and Cl/Ti ratios of the glasses to non-volatile subduction proxies (e.g., Rb/Th, Ba/Nb) of the glasses. Kent et al. (2002) showed that arc lavas unaffected by assimilation of Cl-rich material have Cl/K ratios that correlate with subduction proxies; and such trends represent the addition of subduction components to the melt (Fig. 3d). Any deviation from that trend is related to assimilation of seawater-derived or chlorine-rich brines. The lack of clear positive correlation between Cl/K and Ba/Nb ratios (Fig. 3d) and Cl/Ti and Rb/Th (Appendix C) in the melt inclusions and glassy rinds suggest that SEMFR glasses may have been affected by assimilation of Cl-rich material. In addition, the Cl–K_2O–H_2O systematics (Appendix Fig. C1b) suggests that the contaminant was altered basaltic crust or seawater (Kent et al., 2002).

5.1.3. Least degassed volatile contents

SEMFR glassy rinds and melt inclusions show variable volatile compositions. Olivine-hosted melt inclusions span a wide range in contents of CO_2 (54 to 539 ppm), Cl (111 to 636 ppm), S (601 to 963 ppm), and F (58 to 136 ppm). Probably CO_2 and S contents have been affected by degassing and Cl contents by assimilation. Water contents in the melt inclusions range from 1.33 to 2.32 wt%. Minimally degassed volatile contents of the SEMFR glassy rind falls within this range (CO_2 = 51 ppm, Cl = 447 ppm, S = 898 ppm, H_2O = 2.04 wt%), although F content (186 ppm) is higher than that in associated melt inclusions (Fig. 3a–b). These water estimates represent minimum water content for SEMFR, as wet magma loses their dissolved water upon ascent.

Water contents of the SEMFR melt inclusions and glassy rinds fall within the compositional range of water observed in other arc systems, filtered for degassing using the same approach as for SEMFR glasses for consistency: 1.57–5.00 wt% H_2O in Central America, 0.15–5.97 wt% H_2O in Antilles, 0.40–5.70 wt% H_2O in Mexico, 0.03–3.59 wt% H_2O in Cascades, 0.91–6.46 wt% H_2O in Aleutians–Alaska, 1.00–5.32 wt% H_2O in Kamchatka and 0.19–6.14 wt% H_2O in Marianas (details and references for the arc glasses are reported in Appendix D). In terms of averages, water contents of SEMFR glassy rinds and melt inclusions (1.85 ± 0.26 wt% H_2O) fall at the low end of the range of other arc glasses (Table 1; Plank et al., 2013), within one standard deviation error (1σ), except for the glasses from the Kamchatka arc with the highest mean water content. They also have similar water contents to those of the Mariana Trough backarc basin basaltic (BABB) glass (H_2O = 0.20–2.78 wt%).

5.2. Genesis of SEMFR olivine-hosted melt inclusions

SEMFR melt inclusions are fully enclosed by large (>1 mm) Mg-rich olivines ($Fo_{90–93}$; Ribeiro et al., 2013b) that have a Fe-rich reaction rim indicating disequilibrium with their host melt (Figs. 2c, 6a). They also hosts chromian spinel (Cr# ≥ 50; Ribeiro et al., 2013b; Fig. 2a) and the Fo and CaO contents of their disequilibrium rim overlap the contents of the groundmass phenocrysts (<1 mm; Figs. 2c, 6a), suggesting that the olivine hosts are xenocrysts (Ribeiro et al., 2013b). Olivine – spinel assemblages plot in the mantle array (Arai, 1994) and in the compositional field of Mariana forearc mantle peridotites (Ohara and Ishii, 1998), suggesting that the olivine xenocrysts are derived from harzburgitic forearc mantle (Ribeiro et al., 2013b). The contrasting compositions of major and trace elements between the melt inclusions and their host glasses suggest that they record different magmatic and subduction processes. Here, we discuss the magma genesis of the SEMFR melt inclusions by using trace element ratios, melt thermobarometry (Lee et al., 2009) and Fe_8 content.

We can evaluate the nature of the mantle source of the melt inclusions by using ratios of elements with contrasting incompatibility for the melt. Ratios of a high field strength element (e.g., Nb, Ta, Ti, Zr, Hf), strongly mobilized with the melt, over Yb and Y, that have slightly higher mantle–melt partition coefficient, represent good proxies to track the mantle source composition (Elliott et al., 1997; Gill, 1981; Hawkesworth et al., 1991; McCulloch and Gamble, 1991; Pearce et al., 2005). For example, Nb/Yb ∼ 0.6–0.7 reflects a moderately depleted mantle source like that beneath mid-ocean ridges, while Nb/Yb >> 1 defines an enriched mantle source like that of hot spots and Nb/Yb << 1 reflects a depleted mantle source (e.g., Escrig et al., 2009; Pearce et al., 2005), such as forearc mantle. SEMFR basaltic glasses have Nb/Yb ratios (0.3–1.0) that plot within the compositional field of the Mariana backarc basalts (Nb/Yb = 0.4–2.5), suggesting that they formed by melting of a BABB-like, moderately depleted asthenospheric mantle (Ribeiro et al., 2013a). In contrast, SEMFR melt inclusions, with the exception of one melt inclusion (Nb/Yb = 0.7), record the lowest Nb/Yb (0.1–0.2) yet documented for the Mariana arc-backarc basin system (Fig. 6b), demonstrating that they formed from a more depleted mantle source. In addition, the melt

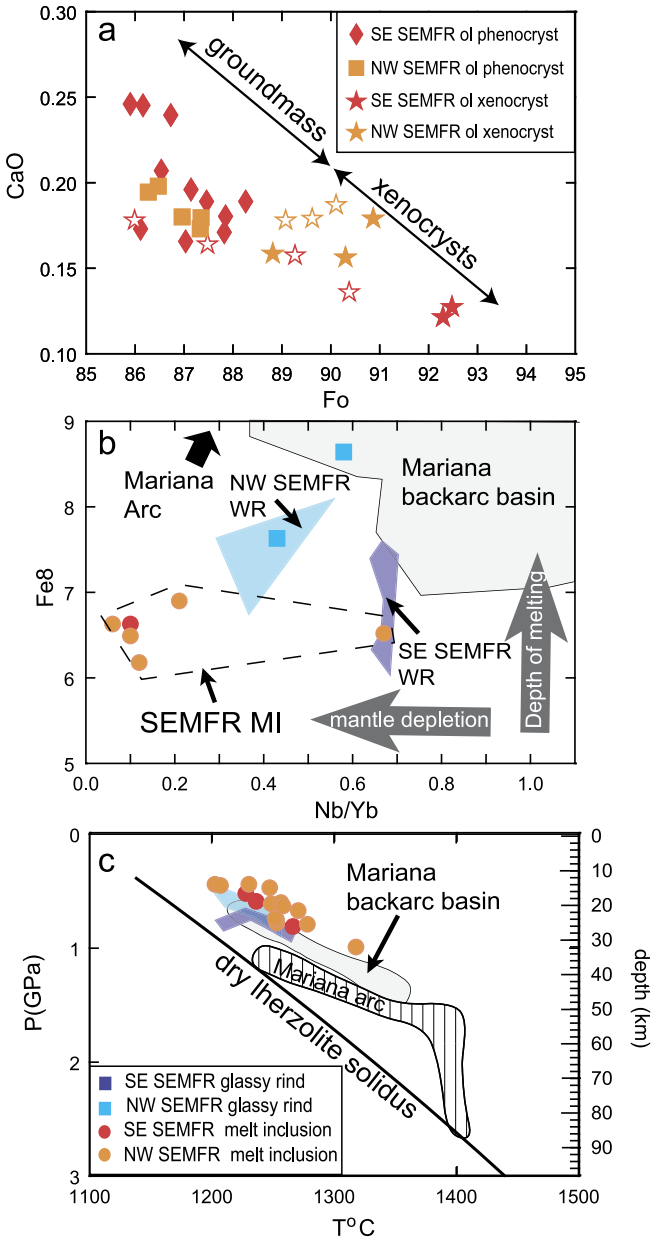

Fig. 6. a) Fo-CaO trend used to discriminate the composition of the groundmass olivines from the mantle olivine xenocrysts. Core composition of the olivine phenocrysts ($Fo_{86–88}$; CaO > 0. 15 wt%) and xenocrysts ($Fo_{90–93}$; CaO < 0.20 wt%; denoted as filled stars) do not overlap. Overlapping between the composition of the xenocrysts rims (empty stars) and the olivine groundmass suggests that the mantle olivines are in disequilibrium with their host melt. Compositions of the olivine are averaged for each grain ($n \geq 2$). Data are from (Ribeiro et al., 2013b). b–c) Conditions of formation of the SEMFR olivine-hosted melt inclusions. b) SEMFR melt inclusions have the lowest Nb/Yb and Fe_8 ever recorded in the Mariana intraoceanic arc, demonstrating that the SEMFR melt inclusions (MI) formed from forearc mantle melting at shallow depth. c) SEMFR melt inclusions have similar P–T conditions of mantle–melt equilibration (Lee et al., 2009) to those of the Mariana backarc basin (BAB) lavas, demonstrating that SEMFR melt inclusions formed at ~22 ± 6.6 km depth (mean 1258 ± 40 °C; 0.67 ± 0.2 GPa) by adiabatic decompression melting of the forearc mantle fluxed by slab fluids. The lherzolite solidus is from Katz et al. (2003). We used $Fe^{3+}/Fe_T = 0.17$ for the Mariana Trough basalts and SEMFR lavas as they have a BABB-like geochemical signature (Ribeiro et al., 2013a, 2013b), and 0.25 for Mariana arc basalts (Kelley and Cottrell, 2009). WR: whole rock.

inclusions cannot represent the primary magma of the host basalt because they are too depleted in Nb and too enriched in Large-Ion Lithophile Elements (LILE: Ba, Sr, Rb, Cs, Sr, K, Pb) relative to their host glass. Fig. 5b shows that the least Nb-depleted melt inclusion is too enriched in LILE to account for the composition of its host glass.

P–T conditions of the primary melt in equilibrium with the mantle wedge can be constrained for primitive glasses (MgO ≥ 7 wt%; Fig. 4) by using the water-sensitive geothermobarometer of Lee et al. (2009). Estimated P–T conditions are those of the last melt in equilibrium with the mantle or mean P–T conditions of polybaric, fractional pooled melts recorded along a melting column (Kelley et al., 2010). To assess the P–T conditions of mantle–melt equilibrium of SEMFR glasses, we used $Fe^{3+}/Fe_T = 0.17$ (Kelley and Cottrell, 2009) along with a BABB-like, moderately depleted mantle source (Fo_{90}) for the host basaltic glasses (Ribeiro et al., 2013b) and a depleted forearc mantle source (Fo_{92}) for the olivine-hosted melt inclusions. It is reasonable to set the Fo content of the mantle source to the maximum Fo content of the SEMFR olivine mantle xenocrysts, since peridotites sampled in the southern Mariana forearc have olivine crystals with $Fo_{90–92}$ (Ohara and Ishii, 1998). Varying the Fo content in the mantle source from Fo_{90} to Fo_{92} affects the temperature by less than 90 °C (1σ) and the pressure by less than 0.5 GPa (1σ). Also, the effect of varying Fe^{3+}/Fe_T from 0.17 to 0.25 is minor on the P–T conditions ($1\sigma \leq 25$ °C for the temperature and $1\sigma \leq 0.1$ GPa for the pressure). Our P–T estimates show that SEMFR olivine-hosted melt inclusions record slightly shallower and cooler P–T conditions of mantle–melt equilibration (mean 1258 ± 40 °C, 0.67 ± 0.2 GPa) than do their host lavas (mean 1287 ± 40 °C; 0.88 ± 0.2 GPa). Such P–T conditions are similar to those recorded by Mariana Trough glassy rinds (mean 1272 ± 40 °C, 0.96 ± 0.2 GPa; Fig. 6c). In contrast, arc lavas (mean 1339 ± 40 °C, 1.65 ± 0.2 GPa) record deeper and warmer P–T conditions of hydrous mantle melting (Kelley et al., 2010).

We can also track the depth of mantle melting by using the Fe_8 content of the least fractionated SEMFR rocks (MgO ≥ 7 wt%; Fig. 4), calculated with the equations of Klein and Langmuir (1987). The effect of PEC correction on Fe_8 is evaluated in Appendix Fig. B2c. Because Mariana arc and backarc lavas started crystallizing plagioclase and clinopyroxene at MgO = 5–6 wt% (e.g., Kelley et al., 2010; Langmuir et al., 2006; Taylor and Martinez, 2003), we are confident that lavas filtered for MgO ≥ 7 wt% for consistency have only crystallized olivine. The shallow melting depth of SEMFR melt inclusions is also illustrated by their lower Fe_8 relative to their host lavas and to the Mariana arc-backarc lavas (Fig. 6b), suggesting that the melt inclusions are shallow mantle melts formed by adiabatic decompression melting of hot asthenospheric mantle wedge fluxed by slab-derived fluids (Fig. 6c).

Composition of the melt inclusions along with melt thermobarometry suggests that SEMFR melt inclusions and their host lavas recorded different magmatic events. Melt inclusions formed by shallow decompression and hydrous melting of a depleted forearc mantle source, while the host lavas formed slightly deeper from a moderately depleted mantle source fluxed by subduction components. Such isolated melt inclusions may have formed when forearc mantle olivine neoblasts captured hydrous melts that metasomatized the forearc mantle (Schiano et al., 1995) at ~22.0 ± 6.6 km depth. To account for our observations, we propose that Late Neogene stretching of the Eocene forearc lithosphere allowed depleted subforearc asthenosphere to melt by adiabatic decompression accompanied by flux mantle melting triggered by dehydration of the shallow Pacific slab (Fig. 7). As the forearc lithosphere continued to stretch 3.7–2.7 Ma ago, less depleted BABB-like asthenospheric mantle flowed beneath the forearc, resulting in formation of the SEMFR basaltic melts (Ribeiro et al., 2013a, 2013b). Basalts captured the forearc mantle xenocrysts upon ascent (Fig. 7b). Previous work on mantle olivines has also shown that their melt inclusions trapped hydrous melts in equi-

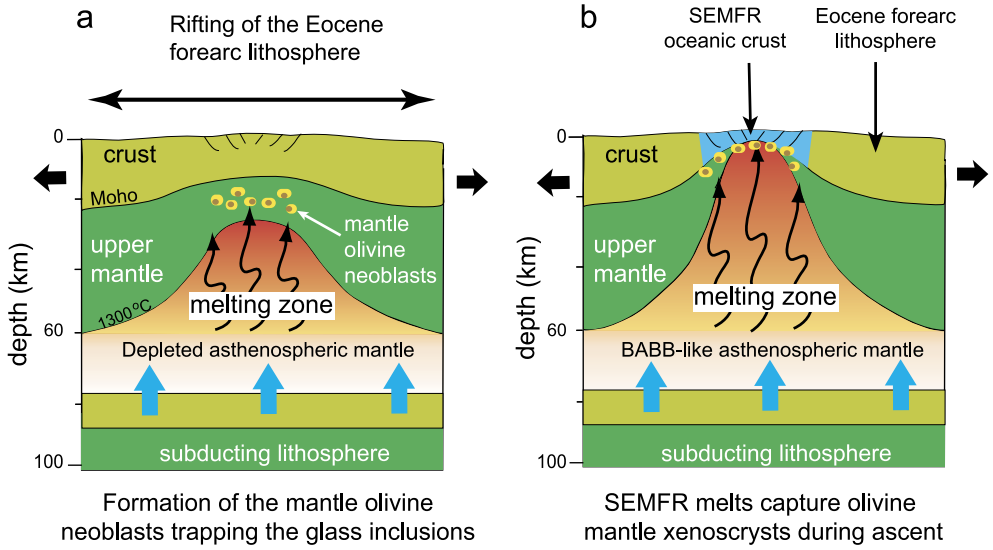

Fig. 7. Magma genesis of SEMFR olivine-hosted melt inclusions. a) Stretching of the Eocene forearc lithosphere triggers melting of the depleted subforearc mantle. Melts captured the shallow, slab-derived fluids (thick blue arrows) before rising into the upper mantle wedge (black curved arrows), forming mantle olivine neoblasts (yellow ellipsoids) that trapped the melt inclusions (brown circle inside the olivine) at ~22 ± 6.6 km depth (see Fig. 6c). b) Further stretching of the forearc lithosphere opens SEMFR and allows less depleted BABB-like mantle to flow beneath SEMFR (Ribeiro et al., 2013a, 2013b). BABB-like asthenospheric mantle is fluxed by the slab-derived fluids and melts by adiabatic decompression to form new oceanic crust in the South Mariana forearc. SEMFR melts captured some forearc mantle olivine neoblasts hosting the melt inclusions during their ascent. (For interpretation of the references to color in this figure legend, the reader is referred to the web version of this article.)

librium with the mantle wedge (Ertan and Leeman, 1999; Schiano et al., 1995). However, it is worth noting that olivine xenocrysts from the forearc mantle hosting melt inclusions have not previously been reported (e.g., Kelley et al., 2010; Shaw et al., 2008; Tamura et al., 2014).

5.3. Composition of shallow slab-derived fluids

SEMFR olivine-hosted melt inclusions represent hydrous melts that captured the subduction outfluxes released beneath forearcs. Therefore, they provide unique insights into the shallowest subduction processes. The composition of the shallow slab fluids were previously assessed based on the composition of serpentinites and serpentinized peridotites from the forearc (e.g., Bebout et al., 2007; Ryan and Chauvel, 2014; Savov et al., 2007). However, the composition of the fluid-mobile elements (e.g., Rb, Ba, Sr, Pb, U) of such rocks are easily modified by alteration (Hart, 1969; Hart et al., 1974; Kelley et al., 2003; Staudigel and Hart, 1983). In contrast, SEMFR melt inclusions and glassy rinds provide a more reliable estimate of the composition of the shallow subduction input, especially as melt inclusions are protected from alteration and degassing (Schiano, 2003).

To track the composition of the water-rich aqueous fluids released during subduction, volatile and fluid-mobile element (e.g., Rb, Cs, Ba, H_2O, Cl, Th) abundances in glasses need to be corrected for fractionation and melting by normalization to a much less fluid-mobile element with a similar mantle–melt partition coefficient (e.g., Nb, Yb, Ce, La; Elliott et al., 1997; Gill, 1981; Hawkesworth et al., 1991; McCulloch and Gamble, 1991; Pearce et al., 2005). Because Th is also mobilized with the solute-rich fluids released during sediment melting (Elliott et al., 1997; Johnson and Plank, 1999; Manning, 2004), the ratios of the other fluid-mobile elements over Th are good proxies to track the shallow aqueous fluids only (Brenan et al., 1995; Elliott et al., 1997; Hawkesworth et al., 1991; Pearce et al., 2005). SEMFR melt inclusions record distinctly higher water and alkali ratios (i.e., H_2O/Ce, Rb/Th, Cs/Th) relative to their host basaltic glassy rinds and to the averaged arc lavas (Fig. 8; Table 1), demonstrating that the melt inclusions captured water- and alkali-rich fluids released from the shallow part of the subducting plate. However, the Ba/Th compositional range of the SEMFR melt inclusions overlaps the averaged ratios of the Mariana, Tonga, Cascades and Central America arc systems (Fig. 8), suggesting that Ba is decoupled from the alkalis during shallow subduction processes.

SEMFR olivine-hosted melt inclusions suggest a compositional gradient in fluid markers, increasing away from the trench (Fig. 8b–c; Table 1). This compositional gradient is also observed in Rb/Th and Cs/Th in the SEMFR host glasses (Fig. 8a; Ribeiro et al., 2013a). Fluid markers peak at ~70–80 km slab depth, demonstrating that the subducting plate mostly dehydrates at depths shallower than beneath the arc magmatic front in cold subduction zones. Also, the high H_2O/Ce ratios observed in SEMFR lavas indicates that the slab surface temperature beneath forearcs is likely sub-solidus (<700 °C; Cooper et al., 2012; Plank et al., 2009), suggesting that such shallow outfluxes are solute-poor aqueous fluids. Our results demonstrate that the downgoing minerals carrying water and alkalis (i.e., serpentinite, amphibole, chlorite, barite, phengite) mostly break down at depths of ~70–80 km to release their water- and alkali-rich aqueous fluids beneath the forearc (Figs. 8c, 9; Bebout et al., 2007; Hattori and Guillot, 2003; Schmidt and Poli, 1998; Tatsumi, 1989). At greater slab depths (>70–80 km), the fluids become progressively more enriched in dissolved solutes beneath the arc volcanoes and the BAB spreading center (Johnson and Plank, 1999; Kawamoto et al., 2012; Manning, 2004; Schmidt and Poli, 1998; Figs. 8c, 9).

6. Conclusions

We have documented that glassy rinds and olivine-hosted melt inclusions in SEMFR basalts provide an unusual opportunity to examine the composition of fluids released from the shallow part of the subducting slab. Our results show that cold downgoing plates mostly dehydrate beneath the forearc at ~70–80 km depth. Our findings that subducted slabs beneath forearcs release relatively water- and alkali-rich aqueous fluids have important implications for understanding Earth's geochemical recycling and subduction zone processes. In particular, they provide new constraints for our understanding of depths at which the downgoing plate dehydrates. They support the idea that the thermal state of the downgoing

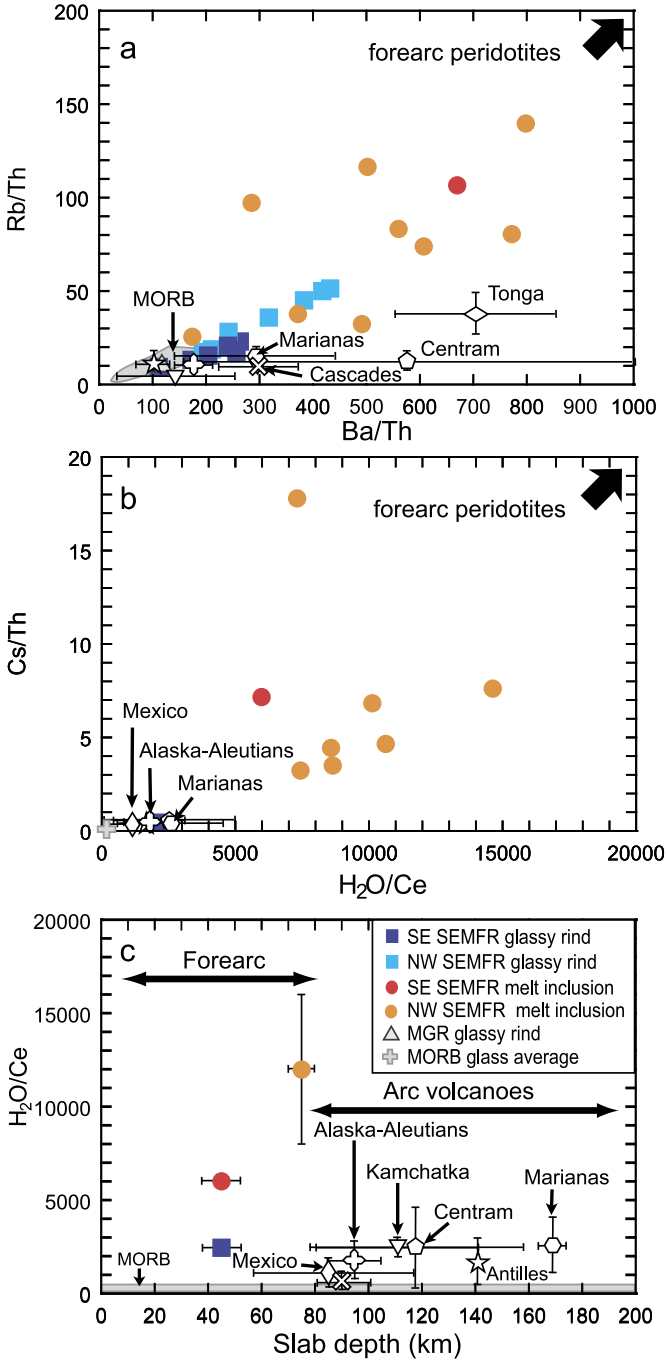

Fig. 8. Composition of the fluids released from the downgoing plate beneath forearcs, compared to the composition of the deeper fluids released beneath arcs. (a) Rb/Th vs Ba/Th and (b) H_2O/Ce vs Cs/Th diagrams. The SEMFR melt inclusions are characterized by a stronger enrichment in Rb/Th, H_2O/Ce and Cs/Th than are their host glassy rinds and the arc lavas (white symbols) from worldwide subduction zones. Composition of the SEMFR glasses trends towards the averaged composition of the South Chamorro peridotites (Kodolányi et al., 2012; Savov et al., 2007). c) H_2O/Ce plotted against slab depth show that the shallow fluids released beneath forearc are the most enriched in subduction-derived water and alkalis, as demonstrated by their highest H_2O/Ce, Rb/Th, Cs/Th. Rb/Th, Ba/Th and Cs/Th follow the same trend as H_2O/Ce with slab depth (Ribeiro et al., 2013a; Table 1). The shallow water- and alkali-rich fluids are mostly released towards the arc volcanoes at ~75 ± 6 km depth to the slab, and the fluids become less enriched in water and fluid-mobile elements as slab depth increase (>80 km). Centram: Central America arc lavas. Today slab depths beneath SEMFR were extrapolated by using the south Mariana slab depths (Becker, 2005; see Fig. 1b). Slab depth at 2.7–3.7 Ma is unknown, and the subducting plate in Miocene time is assumed to be in a similar position as it is today. Averages for the arc volcanoes are reported with one standard deviation error bar. References and filtering details for the arc datasets are reported in Appendix D.

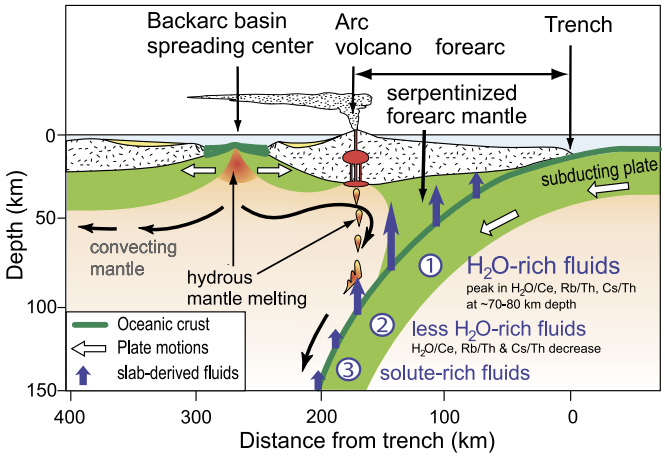

Fig. 9. Sketch of a typical cold subduction zone (Stern, 2002). The downgoing plate releases its fluids (blue arrows) into the mantle wedge as subduction proceeds. Shallow slab-derived fluids are enriched in water, other volatiles and alkalis beneath the forearc (≤80 km slab depth) and they peak at 70–80 km slab depth (1). The fluids contain increasing concentrations of solutes at >80 km depth (2), to become a solute-rich to a supercritical fluid at depth ≥100 km (Johnson and Plank, 1999; Manning, 2004). The shallow water- and alkali-rich fluids generally serpentinize the cold mantle wedge beneath forearcs but help trigger mantle melting beneath SEMFR; while the less water- and alkali-rich fluids trigger hydrous mantle melting deeper, beneath the arc volcanoes and sometimes beneath a backarc basin spreading center.

plate controls the depth of mineral breakdown (Hyndman and Peacock, 2003; Peacock and Wang, 1999; Syracuse et al., 2010; Van Keken et al., 2011; Wada et al., 2008) and hence, the chemical composition of the slab-derived fluids.

Acknowledgements

Two anonymous reviewers and T. Elliott, the editor, provided thorough and helpful reviews that led to significant improvements in the paper. We thank crews of the R/V Yokosuka and the R/V Thomas Thompson for their efforts during YK08-08 Leg 2, YK10-12 and TN273 cruises. We also thank B. Montelone and N. Shimizu (WHOI), T. Grove and A. Andrews (MIT), and M. Lytle (URI) for their help with chemical analyses; E. Schrimsher (UTD) for his help with sample preparation; R.C. Maury (IUEM, Université de Bretagne Occidentale) for his comments; and P. Van Keken (University of Michigan), I. Wada (Tohoku University) and A. Nichols (JAMSTEC) for discussions. This research was supported by the National Science Foundation (grant 0961352 to RJS and grant 0961811 to FM). This is UTD Geosciences contribution # 1266.

Appendix A. Supplementary material

Supplementary material related to this article can be found online at http://dx.doi.org/10.1016/j.epsl.2015.02.018.

References

Andersen, T., Neumann, E.-R., 2001. Fluid inclusions in mantle xenoliths. Lithos 55, 301–320.
Arai, S., 1994. Characterization of spinel peridotites by olivine-spinel compositional relationships: review and interpretation. Chem. Geol. 113, 191–204.
Bebout, G.E., Bebout, A.E., Graham, C.M., 2007. Cycling of B, Li, and LILE (K, Cs, Rb, Ba, Sr) into subduction zones: SIMS evidence from micas in high-P/T metasedimentary rocks. Chem. Geol. 239, 284–304.
Becker, N.C., 2005. Recent Volcanic and Tectonic Evolution of the Southern Mariana Arc. University of Hawai'i, Hawai'i, p. 166.
Brenan, J.M., Shaw, H.F., Ryerson, F.J., Phinney, D.L., 1995. Mineral–aqueous fluid partitioning of trace elements at 900 °C and 2.0 GPa: constraints on the trace element chemistry of mantle and deep crustal fluids. Geochim. Cosmochim. Acta 59, 3331–3350.

Bucholz, C.E., Gaetani, G.A., Behn, M.D., Shimizu, N., 2013. Post-entrapment modification of volatiles and oxygen fugacity in olivine-hosted melt inclusions. Earth Planet. Sci. Lett. 374, 145–155.

Cooper, L.B., Ruscitto, D.M., Plank, T., Wallace, P.J., Syracuse, E.M., Manning, C.E., 2012. Global variations in H_2O/Ce: 1. Slab surface temperatures beneath volcanic arcs. Geochem. Geophys. Geosyst. 13, Q03024. http://dx.doi.org/10.1029/2011gc003902.

Dixon, J.E., Stolper, E.M., 1995. An experimental study of water and carbon dioxide solubilities in mid-ocean ridge basaltic liquids. Part II: applications to degassing. J. Petrol. 36, 1633–1646.

Elliott, T.R., Plank, T., Zindler, A., White, W., Bourdon, B., 1997. Element transport from slab to volcanic front at the Mariana arc. J. Geophys. Res. B, Solid Earth Planets 102, 14991–15019.

Ertan, I.E., Leeman, W.P., 1999. Fluid inclusions in mantle and lower crustal xenoliths from the Simcoe volcanic field, Washington. Chem. Geol. 154, 83–95.

Escrig, S., Bézos, A., Goldstein, S.L., Langmuir, C.H., Michael, P.J., 2009. Mantle source variations beneath the Eastern Lau Spreading Center and the nature of subduction components in the Lau basin–Tonga arc system. Geochem. Geophys. Geosyst. 10, Q04014. http://dx.doi.org/10.1029/2008gc002281.

Fryer, P., Mottl, M., Johnson, L., Haggerty, J., Phipps, S., Maekawa, H., 1995. Serpentine bodies in the forearcs of western Pacific convergent margins: origin and associated fluids. In: Taylor, B., Natland, J. (Eds.), Active Margins and Marginal Basins of the Western Pacific. AGU, Washington, DC, pp. 259–279.

Fujioka, K., Okino, K., Kanamatsu, T., Ohara, Y., 2002. Morphology and origin of the challenger deep in the Southern Mariana Trench. Geophys. Res. Lett. 29, 1372. http://dx.doi.org/10.1029/2001GL013595.

Gaetani, G.A., O'Leary, J.A., Shimizu, N., Bucholz, C.E., Newville, M., 2012. Rapid reequilibration of H_2O and oxygen fugacity in olivine-hosted melt inclusions. Geology 40, 915–918.

Gardner, J.V., Armstrong, A.A., 2011. The Mariana Trench: a new view based on multibeam echosounding. In: AGU Fall Meeting. 2011. American Geophysical Union, San Fransisco, CA. Abstract #OS13B-1517.

Gill, J.B., 1981. Orogenic Andesites and Plate Tectonics. Springer, Berlin Heidelberg.

Grove, T.L., Kinzler, R.J., Bryan, W.B., 1992. Fractionation of mid-ocean ridge basalt (MORB). In: Morgan, J.P., Blackman, D.K., Sinton, J.M. (Eds.), Mantle Flow and Melt Generation at Mid-Ocean Ridges. In: Geophys. Monogr. AGU, Washington, DC, pp. 281–310.

Grove, T.L., Till, C.B., Krawczynski, M.J., 2012. The role of H_2O in subduction zone magmatism. Annu. Rev. Earth Planet. Sci. 40, 413–439.

Hart, S.R., 1969. K, Rb, Cs contents and K/Rb, K/Cs ratios of fresh and altered submarine basalts. Earth Planet. Sci. Lett. 6, 295–303.

Hart, S.R., Erlank, A.J., Kable, E.J.D., 1974. Seafloor basalt alteration: some chemical and Sr isotopic effects. Contrib. Mineral. Petrol. 44, 219–230.

Hattori, K.H., Guillot, S., 2003. Volcanic fronts form as a consequence of serpentinite dehydration in the forearc mantle wedge. Geology 31, 525–528.

Hauri, E.H., 2002. SIMS analysis of volatiles in silicate glasses, 2: isotopes and abundances in Hawaiian melt inclusions. Chem. Geol. 183, 115–141.

Hauri, E.H., Wang, J., Dixon, J.E., King, P.L., Mandeville, C., Newman, S., 2002. SIMS analysis of volatiles in silicate glasses: 1. Calibration, matrix effects and comparisons with FTIR. Chem. Geol. 183, 99–114.

Hawkesworth, C.J., Hergt, J.M., Ellam, R.M., Dermott, F.M., 1991. Element fluxes associated with subduction related magmatism. Philos. Trans. R. Soc. Lond. Ser. A Math. Phys. Eng. Sci. 335, 393–405.

Hyndman, R.D., Peacock, S.M., 2003. Serpentinization of the forearc mantle. Earth Planet. Sci. Lett. 212, 417–432.

Ishizuka, O., Tani, K., Reagan, M.K., Kanayama, K., Umino, S., Harigane, Y., Sakamoto, I., Miyajima, Y., Yuasa, M., Dunkley, D.J., 2011. The timescales of subduction initiation and subsequent evolution of an oceanic island arc. Earth Planet. Sci. Lett. 306, 229–240.

Jochum, K.P., Stoll, B., Herwig, K., Willbold, M., Hofmann, A., Amini, M., Aarburg, S., Abouchami, W., Hellebrand, E., Mocek, B., Raczek, I., Stracke, A., Alard, O., Bouman, C., Becker, S., Dücking, M., Brätz, H., Klemd, R., de Bruin, D., Canil, D., Cornell, D., de Hoog, C.-J., Dalpé, C., Danyushevsky, L.V., Eisenhauer, A., Gao, Y., Snow, J.E., Groschopf, N., Günther, D., Latkoczy, C., Guillong, M., Hauri, E.H., Höfer, H.E., Lahaye, Y., Horz, K., Jacob, D.E., Kasemann, S.A., Kent, A.J.R., Ludwig, T., Zack, T., Mason, P.R.D., Meixner, A., Rosner, M., Misawa, K., Nash, B.P., Pfänder, J., Premo, W.R., Sun, W.D., Tiepolo, M., Vannucci, R., Vennemann, T., Wayne, D., Woodhead, J.D., 2006. MPI-DING reference glasses for in situ microanalysis: new reference values for element concentrations and isotope ratios. Geochem. Geophys. Geosyst. 7, Q02008. http://dx.doi.org/10.1029/2005GC001060.

Johnson, M.C., Plank, T., 1999. Dehydration and melting experiments constrain the fate of subducted sediments. Geochem. Geophys. Geosyst. 1, 1007. http://dx.doi.org/10.1029/1999GC000014.

Kato, T., Beavan, J., Matsushima, T., Kotake, Y., Camacho, J.T., Nakao, S., 2003. Geodetic evidence of back arc spreading in the Mariana Trough. Geophys. Res. Lett. 30, 1625. http://dx.doi.org/10.1029/2002GL016757.

Katz, R.F., Spiegelman, M., Langmuir, C.H., 2003. A new parameterization of hydrous mantle melting. Geochem. Geophys. Geosyst. 4, 1073. http://dx.doi.org/10.1029/2002GC000433.

Kawamoto, T., Kanzaki, M., Mibe, K., Matsukage, K.N., Ono, S., 2012. Separation of supercritical slab-fluids to form aqueous fluid and melt components in subduction zone magmatism. Proc. Natl. Acad. Sci. USA 109, 18695–18700.

Kelley, K.A., Cottrell, E., 2009. Water and the oxidation state of subduction zone magmas. Science 325, 605–607.

Kelley, K.A., Plank, T., Ludden, J., Staudigel, H., 2003. Composition of altered oceanic crust at ODP Sites 801 and 1149. Geochem. Geophys. Geosyst. 4, 8910. http://dx.doi.org/10.1029/2002GC000435.

Kelley, K.A., Plank, T., Newman, S., Stolper, E.M., Grove, T.L., Parman, S.W., Hauri, E.H., 2010. Mantle melting as a function of water content beneath the Mariana Arc. J. Petrol. 51, 1711–1738.

Kent, A.J.R., 2008. Melt inclusions in basaltic and related volcanic rocks. Rev. Mineral. Geochem. 69, 273–331.

Kent, A.J.R., Peate, D.W., Newman, S., Stolper, E.M., Pearce, J.A., 2002. Chlorine in submarine glasses from the Lau Basin: seawater contamination and constraints on the composition of slab-derived fluids. Earth Planet. Sci. Lett. 202, 361–377.

Klein, E.M., Langmuir, C.H., 1987. Global correlations of ocean ridge basalt chemistry with axial depth and crustal thickness. J. Geophys. Res. 92, 8089–8115.

Kodolányi, J., Pettke, T., Spandler, C., Kamber, B.S., Gméling, K., 2012. Geochemistry of ocean floor and fore-arc serpentinites: constraints on the ultramafic input to subduction zones. J. Petrol. 53, 235–270.

Langmuir, C.H., Bezos, A., Escrig, S., Parman, S.W., 2006. Chemical systematics and hydrous melting of the mantle in back-arc basins. In: Christie, D.M., et al. (Eds.), Back-Arc Spreading Systems: Geological, Biological, Chemical, and Physical Interactions. In: Geophys. Monogr. AGU, Washington, DC, pp. 87–146.

Le Bas, M.J., 2000. IUGS reclassification of the high-Mg and picritic volcanic rocks. J. Petrol. 41, 1467–1470.

Lee, C.-T.A., Luffi, P., Plank, T., Dalton, H., Leeman, W.P., 2009. Constraints on the depths and temperatures of basaltic magma generation on Earth and other terrestrial planets using new thermobarometers for mafic magmas. Earth Planet. Sci. Lett. 279, 20–33.

Manning, C.E., 2004. The chemistry of subduction-zone fluids. Earth Planet. Sci. Lett. 223, 1–16.

Martinez, F., Fryer, P., Sleeper, J., Stern, R.J., Kelley, K., Ohara, Y., Ribeiro, J., 2014. Hydrous lithosphere and diffuse crustal accretion and tectonics in the southern Mariana margin: a possible analog for subduction zone infancy. In: Fall Meeting 2014. American Geophysical Union. Abstract # T52B-03.

McCulloch, M.T., Gamble, J.A., 1991. Geochemical and geodynamical constraints on subduction zone magmatism. Earth Planet. Sci. Lett. 102, 358–374.

Meijer, A., Reagan, M.K., 1981. Petrology and geochemistry of the island of Sagrigan in the Mariana arc: calc-alkaline volcanism in an oceanic setting. Contrib. Mineral. Petrol. 77, 337–354.

Newman, S., Lowenstern, J.B., 2002. VolatileCalc: a silicate melt–H_2O–CO_2 solution model written in Visual Basic for excel. Comput. Geosci. 28, 597–604.

Ohara, Y., Ishii, T., 1998. Peridotites from the southern Mariana forearc: heterogeneous fluid supply in mantle wedge. Isl. Arc 7, 541–558.

Peacock, S.M., Wang, K., 1999. Seismic consequences of warm versus cool subduction metamorphism: examples from Southwest and Northeast Japan. Science 286, 937–939.

Pearce, J.A., Stern, R.J., Bloomer, S.H., Fryer, P., 2005. Geochemical mapping of the Mariana arc-basin system: implications for the nature and distribution of subduction components. Geochem. Geophys. Geosyst. 6, Q07006. http://dx.doi.org/10.1029/2004GC000895.

Peccerillo, A., Taylor, S.R., 1976. Geochemistry of Eocene calcalkaline volcanic rocks from the Kastamonu Area, Northern Turkey. Contrib. Mineral. Petrol. 58, 63–81.

Plank, T., Cooper, L.B., Manning, C.E., 2009. Emerging geothermometers for estimating slab surface temperatures. Nat. Geosci. 2, 611–615.

Plank, T., Kelley, K.A., Zimmer, M.M., Hauri, E.H., Wallace, P.J., 2013. Why do mafic arc magmas contain ~4 wt% water on average? Earth Planet. Sci. Lett. 364, 168–179.

Reagan, M.K., McClelland, W.C., Girard, G., Goff, K.R., Peate, D.W., Ohara, Y., Stern, R.J., 2013. The geology of the southern Mariana fore-arc crust: implications for the scale of Eocene volcanism in the western Pacific. Earth Planet. Sci. Lett. 380, 41–51.

Ribeiro, J., Stern, R.J., Kelley, K., Martinez, F., Ishizuka, O., Manton, W.I., Ohara, Y., 2013a. Nature and distribution of the slab-derived fluids and the mantle source along the Southeast Mariana forearc rift. Geochem. Geophys. Geosyst. 14, 4585–4607. http://dx.doi.org/10.1002/ggge.20244.

Ribeiro, J., Stern, R.J., Martinez, F., Ishizuka, O., Merle, S.G., Kelley, K.A., Anthony, E.Y., Ren, M., Ohara, Y., Reagan, M., Girard, G., Bloomer, S.H., 2013b. Geodynamic evolution of a forearc rift in the southernmost Mariana Arc. Isl. Arc 22, 453–476.

Roeder, P.L., Emslie, R.F., 1970. Olivine–liquid equilibrium. Contrib. Mineral. Petrol. 29, 275–289.

Ruscitto, D.M., Wallace, P.J., Cooper, L.B., Plank, T., 2012. Global variations in H_2O/Ce: 2. Relationships to arc magma geochemistry and volatile fluxes. Geochem. Geophys. Geosyst. 13, Q03025. http://dx.doi.org/10.1029/2011gc003887.

Ryan, J.G., Chauvel, C., 2014. The subduction-zone filter and the impact of recycled materials on the evolution of the mantle. In: Holland, H.D., Turekian, K.K. (Eds.), The Mantle and Core, vol. 3, Treatise on Geochemistry. 2nd edition. Elsevier, Oxford, pp. 479–508.

Savov, I.P., Ryan, J.G., D'Antonio, M., Fryer, P., 2007. Shallow slab fluid release across and along the Mariana arc-basin system: insights from geochemistry of serpentinized peridotites from the Mariana fore arc. J. Geophys. Res. 112, B09205. http://dx.doi.org/10.1029/2006JB004749.

Scaillet, B., Pichavant, M., 2003. Experimental constraints on volatile abundances in arc magmas and their implications for degassing processes. In: Special Publications, vol. 213. Geological Society, London, pp. 23–52.

Schiano, P., 2003. Primitive mantle magmas recorded as silicate melt inclusions in igneous minerals. Earth-Sci. Rev. 63, 121–144.

Schiano, P., Bourdon, B., 1999. On the preservation of mantle information in ultramafic nodules: glass inclusions within minerals versus interstitial glasses. Earth Planet. Sci. Lett. 169, 173–188.

Schiano, P., Clocchiatti, R., Shimizu, N., Maury, R.C., Jochum, K.P., Hofmann, A.W., 1995. Hydrous, silica-rich melts in the sub-arc mantle and their relationship with erupted arc lavas. Nature 377, 595–600.

Schmidt, M., Poli, S., 1998. Experimentally based water budgets for dehydrating slabs and consequences for magma generation. Earth Planet. Sci. Lett. 163, 361–379.

Shaw, A.M., Hauri, E.H., Fischer, T.P., Hilton, D.R., Kelley, K.A., 2008. Hydrogen isotopes in Mariana arc melt inclusions: implications for subduction dehydration and the deep-Earth water cycle. Earth Planet. Sci. Lett. 275, 138–145.

Shaw, A.M., Hauri, E.H., Behn, M.D., Hilton, D.R., Macpherson, C.G., Sinton, J.M., 2012. Long-term preservation of slab signatures in the mantle inferred from hydrogen isotopes. Nat. Geosci. 5, 224–228.

Sisson, T.W., Layne, G.D., 1993. H_2O in basalt and basaltic andesite glass inclusions from four subduction-related volcanoes. Earth Planet. Sci. Lett. 117, 619–635.

Smith, W.H.F., Wessel, P., 1990. Gridding with continuous curvature splines in tension. Geophysics 55, 293–305.

Staudigel, H., Hart, S.R., 1983. Alteration of basaltic glass: mechanisms and significance for the oceanic crust-seawater budget. Geochim. Cosmochim. Acta 47, 337–350.

Stern, R.J., 2002. Subduction zones. Rev. Geophys. 40, 37. http://dx.doi.org/10.1029/2001RG000108.

Straub, S.M., Layne, G.D., 2003. Decoupling of fluids and fluid-mobile elements during shallow subduction: evidence from halogen-rich andesite melt inclusions from the Izu arc volcanic front. Geochem. Geophys. Geosyst. 4, 9003. http://dx.doi.org/10.1029/2002gc000349.

Sun, S.S., McDonough, W.F., 1989. Chemical and isotopic systemics of ocean basalt: implications for mantle composition and processes. In: Saunders, A.D., Norry, M.J. (Eds.), Magmatism in the Ocean Basins. Geological Society of London, Special Publications, London, pp. 313–345.

Syracuse, E.M., Van Keken, P.E., Abers, G.A., 2010. The global range of subduction zone thermal models. Phys. Earth Planet. Inter. 183, 73–90.

Tamura, Y., Ishizuka, O., Stern, R.J., Nichols, A.R.L., Kawabata, H., Hirahara, Y., Chang, Q., Miyazaki, T., Kimura, J., Embley, R.W., Tatsumi, Y., 2014. Mission immiscible: distinct subduction components generate two primary magmas at pagan volcano, Mariana arc. J. Petrol. 55, 63–101.

Tatsumi, Y., 1989. Migration of fluid phase and genesis of basalt magmas in subduction zones. J. Geophys. Res., Solid Earth 94, 4697–4707.

Taylor, B., Martinez, F., 2003. Back-arc basin basalt systematics. Earth Planet. Sci. Lett. 210, 481–497.

Van Keken, P.E., Hacker, B.R., Syracuse, E.M., Abers, G.A., 2011. Subduction factory: 4. Depth-dependent flux of H_2O from subducting slabs worldwide. J. Geophys. Res., Solid Earth 116, B01401. http://dx.doi.org/10.1029/2010jb007922.

Wada, I., Wang, K., He, J., Hyndman, R.D., 2008. Weakening of the subduction interface and its effects on surface heat flow, slab dehydration, and mantle wedge serpentinization. J. Geophys. Res., Solid Earth 113, B04402. http://dx.doi.org/10.1029/2007jb005190.

Wade, J.A., Plank, T., Melson, W.G., Soto, G.J., Hauri, E.H., 2006. The volatile content of magmas from Arenal volcano, Costa Rica. J. Volcanol. Geotherm. Res. 157, 94–120.

Webster, J.D., Botcharnikov, R.E., 2011. Distribution of sulfur between melt and fluid in S–O–H–C–Cl–bearing magmatic systems at shallow crustal pressures and temperatures. Rev. Mineral. Geochem. 73, 247–283.

Wessel, P., Smith, W.H.F., 1995. New version of the Generic Mapping Tools released. Eos Trans. AGU 76, 329.

Wessel, P., Smith, W.H.F., 1998. New, Improved Version of Generic Mapping Tools Released. Eos Trans. AGU 79, 579.